Influence of double Auger decay on low-energy 3*d* photoelectrons of krypton

S. Sheinerman,[1,2,*] P. Linusson,[3] J. H. D. Eland,[2,4] L. Hedin,[2] E. Andersson,[2] J.-E. Rubensson,[2] L. Karlsson,[2] and R. Feifel[2,†]

[1]*Department of Physics, St. Petersburg State Maritime Technical University, 198262 St. Petersburg, Russia*

[2]*Department of Physics and Astronomy, Uppsala University, Box 516, SE-751 20 Uppsala, Sweden*

[3]*Department of Physics, Stockholm University, AlbaNova University Centre, SE-106 91 Stockholm, Sweden*

[4]*Department of Chemistry, Physical and Theoretical Chemistry Laboratory, Oxford University, South Parks Road, Oxford OX1 3QZ, United Kingdom*

(Received 22 May 2012; published 23 August 2012)

Effects of postcollision interaction (PCI) observable in low-energy 3*d* photoelectron spectra of Kr, which are associated with double Auger decay of the created inner-shell vacancy, are investigated by a combined experimental and theoretical approach. Measurements are based on an efficient multielectron coincidence method. Calculations have been carried out in the framework of a semiclassical approach. Our investigation reveals strong PCI distortion of the photoelectron line shapes, which depends on the kinematics of the process and the characteristics of the double Auger decay.

DOI: 10.1103/PhysRevA.86.022515 PACS number(s): 33.70.Ca, 33.80.Eh, 34.50.Gb

I. INTRODUCTION

Radiationless decay of atomic inner-shell vacancies created by photoionization occurs by means of single or multiple Auger electron emission. Core-level photoionization followed by single Auger decay has been studied for many years. Particular attention has been paid to the influences of Auger decay on the photoelectron spectra, which are quite well documented both experimentally and theoretically (see, for instance, the reviews provided by Refs. [1,2]).

The first experimental evidence of a double Auger (DA) process was reported by Carlson and Krause [3,4] in the mid-1960s. Recent development of experimental coincidence techniques for efficient detection of several electrons [5–8] allows one to register reliably events which involve multiple Auger decay. Emission of two or several Auger electrons is expected to affect the energy and angular distribution of the emitted photoelectron. In particular, postcollision interaction (PCI) manifests itself in spectra of photoelectrons or Auger electrons.

PCI can be thought of as a special kind of electron correlation process associated with the interaction of charged particles of a resonant process, comprising the creation and decay of an intermediate quasistationary state. In the case of inner-shell photoionization followed by DA decay, PCI implies the interaction of the emitted photoelectron with the two subsequent Auger electrons and with the field of the ion, which varies during the Auger decay. Previously, PCI effects in DA processes have been investigated experimentally by means of threshold photoelectron yields measured in the vicinity of inner-shell vacancies: Kr $1s^{-1}$, Kr $2p^{-1}$, Kr $3p^{-1}$, Ar $1s^{-1}$, Ar $2p^{-1}$, Xe $4p^{-1}$, and Xe $4d^{-1}$ [9–18]. Also an investigation of PCI-distorted photoelectron lines associated with DA decay and measured in coincidence with the two ejected Auger electrons has been carried out more recently for the case of Ar $2p$ photoionization [19].

From a theoretical point of view there are a number of PCI models to describe the effects occurring within DA processes: (1) a classical model to describe the release of threshold electrons [12], (2) a classical model to take into account cascade Auger decay [20], (3) a quantum-mechanical eikonal approach to the DA processes [21,22], and (4) a semiclassical approach to the DA processes formulated very recently by Gerchikov and Sheinerman [23]. These models allow one to describe adequately experimental results in the range where their applicability conditions are fulfilled.

In this work, we investigate PCI effects observable in low-energy photoelectron spectra of Kr measured for 3*d* inner-shell ionization and influenced by subsequent DA decay. There are several reasons for carrying out such an investigation: First, PCI is expected to affect low-energy photoelectrons strongly, and the associated spectra cannot be analyzed without taking such influences into account. Second, recent studies on the DA decay of the Kr 3*d* vacancies [24,25] revealed different pathways for this process. In particular, the DA decay in the case of Kr 3*d* occurs mainly through a cascade double Auger (CDA) decay where the electrons are emitted stepwise through the creation and decay of an intermediate quasistationary state. Analysis of the Auger electron spectra has revealed important parameters of these intermediate states and energies of the ejected Auger electrons. These energies are found to be comparatively small, i.e., on the order of a few eVs, and comparable with the energies of the photoelectrons. Hence the interaction between the photoelectron and the Auger electrons is expected to be strong and contribute noticeably to the distortion of spectral line shapes. Apart from the CDA pathway, for some of the emitted Auger electrons, a direct double Auger (DDA) decay occurs where the two electrons are emitted simultaneously. The DDA pathway contributes also to the PCI distortion of the photoelectron spectra for some selected energies of the Auger electrons. Third, adequate tools both on the experimental and theoretical side have been developed recently to investigate the PCI-distorted low-energy electron spectra. On the experimental side it is in particular the technique of multielectron coincidence spectroscopy based on a magnetic bottle time-of-flight spectrometer [8] which

*sheinerman@post.ru

†raimund.feifel@physics.uu.se

is vital for the present study. Using this method allows one to obtain complete, electronic-state-sensitive, triple-photoionization (TPI) electron spectra over a wide range of kinetic energies [26]. On the theoretical side the semiclassical Wentzel-Kramers-Brillouin (WKB) approach [23] has been employed recently to describe PCI effects in DA processes for low excess energies above the inner-shell threshold. Application of this approach to the case studied here can be considered as a first systematic investigation of four-body PCI effects in the near-threshold region.

This paper presents a combined experimental and theoretical study of low-energy Kr $3d$ photoelectron spectra associated with DA processes. The PCI distortion of these lines proves to be significant. The shifts and broadening of the line shapes are revealed by the coincidence measurements and confirmed by the WKB calculations. The generally good agreement between the measured and calculated line shapes reflects the reliability of the results obtained.

This paper is organized as follows: Sec. II describes our experimental method, and Sec. III describes the theoretical approach used for calculating the cross section of the DA processes. In Sec. IV we compare directly the experimental results to the numerical results and interpret the data accordingly. The atomic system of units $|e| = m_e = \hbar = 1$ is used throughout.

II. EXPERIMENT

The experiments were performed at beam line U49/2 PGM-2 [27] at the BESSY-II storage ring in Berlin. Multielectron coincidence data were recorded using a highly efficient magnetic bottle time-of-flight spectrometer [5,28] capable of resolving individual electron kinetic energies. The resolving power of the apparatus for single electrons can be expressed as a fixed numerical resolution $E/\Delta E$ of about 50 for electron energies above 1 eV and a fixed resolution ΔE of about 20 meV at lower energies.

Commercially obtained Kr gas was let into the interaction region of the spectrometer as an effusive jet from a needle and ionized by soft x-ray photons of monochromatically selected energies in the vicinity of the Kr $3d$ thresholds. The electron flight times were referenced to the synchrotron light pulses, which have a width of ~30 ps and a periodicity of 800.5 ns [29] when BESSY-II is operated in single-bunch mode. In the present study, a fast Auger electron was used to mark the ionizing light pulse and to establish subsequently the absolute flight times of additional electrons originating from the same ionization event. Where this was not possible, because the Auger electron energies were too low, energy conservation was used with the known triple-ionization energies to establish the true time origin of electron triples.

In order to avoid accidental coincidences, the electron count rates were restricted to a small fraction of the light pulse rate. This was achieved by closing the exit slit of the monochromator, whereby the intensity of the synchrotron light was suitably reduced. As a consequence, the energy resolution of the light was not a limiting factor for the measurements. The photon energy was calibrated using literature values of the Kr $3d$ near-edge x-ray absorption spectrum [30], while the time-to-energy conversion was calibrated using known values of Xe and Kr Auger lines [31,32], augmented for low electron energies by the ^2D photoelectron lines of Kr corrected for the PCI shift associated with single Auger decay.

III. THEORETICAL CONSIDERATION OF POSTCOLLISION INTERACTION IN DOUBLE AUGER PROCESSES

We consider the DA decay of a Kr $3d$ vacancy, which can occur either in terms of a DDA process or in terms of a CDA process. In the first case, the reaction scheme leading to a triple vacancy in the $4p$ shell can be summarized as

$$\begin{aligned}\gamma + \mathrm{Kr} &\rightarrow e_1 + \mathrm{Kr}^{+*}\left(3d_{3/2,5/2}^{-1}\right)\\ &\rightarrow e_1(E_1) + e_{1A}(E_2) + e_{2A}(E_3)\\ &\quad + \mathrm{Kr}^{3+}((4p^{-3})\,^4S, {}^2D, {}^2P),\end{aligned} \tag{1}$$

where γ denotes the photon of energy ω, e_1 is the first emitted photoelectron, e_{1A} and e_{2A} are the subsequently emitted Auger electrons 1 and 2, and E_1, E_2, and E_3 are the associated electron kinetic energies, respectively.

In the second case of a CDA process, where the decay involves intermediate Kr^{2+*} states, the corresponding reaction scheme, leading to the same triply ionized final states, can be denoted as

$$\begin{aligned}\gamma + \mathrm{Kr} &\rightarrow e_1 + \mathrm{Kr}^{+*}\left(3d_{3/2,5/2}^{-1}\right) \rightarrow e_1 + e_{1A}(E_2') + \mathrm{Kr}^{2+*}\\ &\rightarrow e_1(E_1) + e_{1A}(E_2) + e_{2A}(E_3)\\ &\quad + \mathrm{Kr}^{3+}((4p^{-3})\,^4S, {}^2D, {}^2P).\end{aligned} \tag{2}$$

In previous works, influences of PCI on the photoelectron yield for both cases (1) and (2) were taken into account within the so-called eikonal approximation [21,22]. This approach is based on the assumption that the interaction of the electrons at large distances contributes mainly to the PCI effect where the kinetic energy of the emitted particles is much larger than their potential energy, i.e., $W_{\mathrm{kin}} \gg W_{\mathrm{pot}}$. Such an approximation is valid for comparatively high kinetic energies of the photoelectron and allows one to describe experimental spectra very well [19]. However, for comparatively low kinetic energy photoelectrons this condition breaks down, and one needs to go beyond the eikonal approximation. To this end, a model for PCI in DA processes was developed very recently using a semiclassical formalism [23] and WKB wave functions for the description of the electron's motion, which takes into account more accurately the interaction of the electrons and which allows one to avoid restrictions of the eikonal model. Hence, for describing the emission of low-kinetic-energy photoelectrons in cases (1) and (2), we will use this new WKB model in the present work.

A. PCI in direct double Auger decay (DDA)

In this case the amplitude A_{DDA} is proportional to the overlap integral I of the photoelectron wave functions of the intermediate and final states:

$$I = \int_0^\infty \chi_{E_1'}^{(+)}(r)\,\chi_{E_1}^{(-)}(r)\,dr\,. \tag{3}$$

The wave functions $\chi^{(+)}$ and $\chi^{(-)}$ have asymptotes of outgoing and ingoing waves, respectively, and E_1' is the complex

energy of the photoelectron in the intermediate state before the Auger decay happens. Here the photoelectron moves in the field of the singly charged ion. After the Auger decay the photoelectron has the velocity V_1 and energy E_1; its motion will be affected by the field of the triply charged ion and by the two Auger electrons of energies E_2 and E_3, respectively.

The photoelectron distribution as a function of kinetic energy ε relative to the unshifted value $E_1^{(0)}$ ($\varepsilon = E_1 - E_1^{(0)}$) has the form [23]

$$P(\varepsilon) = |A_{DDA}|^2 \propto \frac{\Gamma C}{\varepsilon^2 + \frac{\Gamma^2}{4}} \frac{1}{\left[\left(E_1^{(0)} - \frac{\varepsilon}{C}\right)^2 + \frac{\Gamma^2}{4}\left(1 + \frac{1}{C}\right)^2\right]^{1/4}} e^{2\,\mathrm{Im}[\varphi_f(r^*) - \varphi_i(r^*)]}. \tag{4}$$

Here Γ is the width of the $3d$ inner vacancy, and the parameter C takes into account the kinematics of the emitted Auger electrons through their relative velocities V_{12} and V_{13}, respectively:

$$C = 2 - \frac{V_1}{V_{12}} - \frac{V_1}{V_{13}}. \tag{5}$$

The explicit expressions for the phase factors $\varphi_{i,f}(r)$ are given by Gerchikov and Sheinerman [23].

B. PCI in cascade double Auger decay (CDA)

According to Eq. (2), emission of the two Auger electrons occurs, in the cascade case, sequentially through creation and decay of quasistationary states. The first Auger electron is emitted upon the decay of the $3d$ inner-shell vacancy with a width Γ_1, leading to the creation of an intermediate state with a width Γ_2. Decay of this latter state leads to the emission of the second Auger electron. The amplitude of this process, A_{CDA}, can be expressed as an integral over the energy variable u of the product of the two factors, I_1 and I_3, which describe the propagation of the photoelectron and the first Auger electron, respectively:

$$A_{CDA} \propto \int_{-\infty}^{\infty} \frac{du}{2\pi} I_1(u)\, I_3(u). \tag{6}$$

The first factor, I_1, is the product of two independent overlap integrals involving the photoelectron wave functions in different states:

$$I_1(u) = \int_0^{\infty} \chi_1^{(+)}(r_1)\, \chi_2^{(-)}(r_1)\, dr_1 \int_0^{\infty} \chi_2^{(+)}(r_2)\, \chi_3^{(-)}(r_2)\, dr_2. \tag{7}$$

Here χ_1 is the photoelectron wave function in the initial state before the first Auger decay; χ_2 is the photoelectron wave function in the intermediate state after the first Auger decay but before the second Auger decay; χ_3 is the photoelectron wave function in the final state after the second Auger decay. The functions χ_1, χ_2, and χ_3 describe the motion of the photoelectron in the field of the singly charged ion, the doubly charged ion plus the first Auger electron, and the triply charged ion plus the two Auger electrons, respectively.

The second factor, I_3, is the overlap integral of the first Auger electron wave functions χ_4 and χ_5, which describe its motion before and after the second Auger decay, respectively:

$$I_3(u) = \int_0^{\infty} \chi_4^{(+)}(r_3)\, \chi_5^{(-)}(r_3)\, dr_3. \tag{8}$$

Note that the motion of the first Auger electron in the intermediate state is affected by the field of the doubly charged ion plus the photoelectron. In the final state this Auger electron propagates in the field of the triply charged ion plus two electrons, namely, the photoelectron and the second Auger electron.

Integrals I_1 and I_3 are calculated using the WKB approximation for describing the wave functions χ_1 to χ_5. Their precise forms are presented in Ref. [23]. Note that the amplitude A_{CDA} depends on the widths Γ_1 and Γ_2 of the intermediate states involved and the effective charges of the mean-field potentials for the corresponding electronic states. These charges depend on the velocities of the escaping electrons and their direction of motion. For the states of the photoelectron before the first Auger decay, after the first Auger decay, and after the second Auger decay, the effective charges are 1, $2 - V_1/V_{12}$, and $3 - V_1/V_{12} - V_1/V_{13}$, respectively. For the states of the first Auger electron, before and after the second Auger decay, the effective charges are $2 - V_2/V_{12}$ and $3 - V_2/V_{12} - V_2/V_{23}$, respectively. The integration over the energy variable u in Eq. (6) is performed numerically. Subsequent to that the cross section of process (2) is obtained by squaring the modulus of Eq. (6):

$$\frac{d^2\sigma}{d\varepsilon_1\, d\varepsilon_3} = |A_{CDA}(E_1, E_2, E_3)|^2. \tag{9}$$

Here ε_1 and ε_3 are the energies of the photoelectron and the second Auger electron measured relative to their unshifted values, $E_1^{(0)}$ and $E_3^{(0)}$, respectively: $\varepsilon_1 = E_1 - E_1^{(0)}$; $\varepsilon_3 = E_3 - E_3^{(0)}$. Note that due to the energy conservation, $\varepsilon_1 + \varepsilon_2 + \varepsilon_3 = 0$, there are only two independent energies ε_i.

IV. RESULTS AND DISCUSSION

In what follows, we present experimental low-kinetic-energy spectra of photoelectrons emitted from the Kr $3d$ inner shells and compare them directly to our numerical results. Coincidence detection of the photoelectron with one or two of the Auger electrons allows us to select events which are associated with well-defined final ionic states. For detailed analysis and comparison of the measurements with the calculations we have chosen DA decays which lead to the final $Kr^{3+}((4p^{-3})^2P)$ states. Furthermore, we have selected three different incident photon energies for the present study: $\omega_1 = 94.10$ eV, $\omega_2 = 94.55$ eV, and $\omega_3 = 96.0$ eV, which correspond to an electron excess energy of the $3d_{5/2}$ photoelectron of 0.31, 0.76, and 2.21eV, respectively. In the

case of $\omega_3 = 96.0$ eV there is also the possibility for emission of a photoelectron from the $3d_{3/2}$ subshell with an excess energy of 0.96 eV.

The experimental spectra shown below reflect the photoelectron yield measured in coincidence with one of the Auger electrons selected within a certain energy interval, $E_{\min} < E < E_{\max}$. The numerical energy distributions based on Eqs. (4) and (9) were integrated over the same energy window in order to be comparable to the experimental data. In addition to that, the calculated distributions were integrated over the electron emission angles because the experiment detects essentially all electrons emitted into the solid angle of 4π.

Analyzing the Auger electron spectra which lead to the $Kr^{3+}((4p^{-3})^2P)$ states (cf. Refs. [24,25]), we can select three different energy regions with strong intensities of the cascade Auger emission: 0.7–1.2, 4.5–5.5, and 7.0–7.5 eV. For the first region the CDA decay occurs through the emission of a 14.7-eV Auger electron in the first step and a 0.73-eV Auger electron [25] in the second step (according to Ref. [24], the energy of the second Auger electron is 0.65 eV). In the second region the first-step Auger electron has an energy of 4.76 eV [25] (or 5.0 eV according to Ref. [24]), and the second-step Auger electron has an energy of 10.69 eV (or 10.4 eV according to Ref. [24]). In the third region the emission of a 6.75-eV Auger electron [25] (or 7.5 eV [24]) occurs, followed by the emission of the second-step Auger electron of 8.70 eV (or 7.85 eV [24]). Analyzing these intervals, we can investigate the influence of the cascade Auger electrons of different energies on the PCI effects. Apart from this there is a region (1.5–3.9 eV) where the distribution of the emitted electrons reveals an essentially structureless continuum which can be attributed to the DDA process. According to this selection, our measurements and calculations cover coincidence events involving a $3d$ photoelectron and different groups of Auger electron energies which can be attributed to either CDA or DDA processes.

In Fig. 1 we present measured and calculated photoelectron spectra for the photon energies of $\omega_1 = 94.10$ eV [Fig. 1(a)], $\omega_2 = 94.55eV$ [Fig. 1(b)], and $\omega_3 = 96.0$ eV [Fig. 1(c)], which are associated with the emission of a slow 0.73-eV Auger electron in the second step of the CDA decay. The intervals of the selected Auger electrons, which are recorded in coincidence with the photoelectrons, are 0.68–0.89 eV for ω_1, 0.70–0.91 eV for ω_2, and 0.67–0.98 eV for ω_3. For the calculations we used similar energy intervals: 0.70–0.90, 0.725–0.95, and 0.73–0.98 eV, respectively. Note that the theoretical approach [23] has limitations for the region where the energies of the photoelectron and the Auger electron are equal or very close. Our approximation does not work perfectly in this region, and the numerical implementation of the formulas used implies long CPU time for the calculations as well as other complications. Therefore we restricted ourselves to the region where the energies of the photoelectron are less than the energies of the Auger electron. This restriction influences the choice of the theoretical intervals which are close but not equal to the experimental ones. The calculations have been carried out using Eq. (9) with a resonance width $\Gamma_1 \equiv \Gamma(3d_{3/2}) = \Gamma(3d_{5/2}) = 88$ meV [33] and a width of the intermediate state $\Gamma_2 = 73$ meV [25]. Apart from this we used

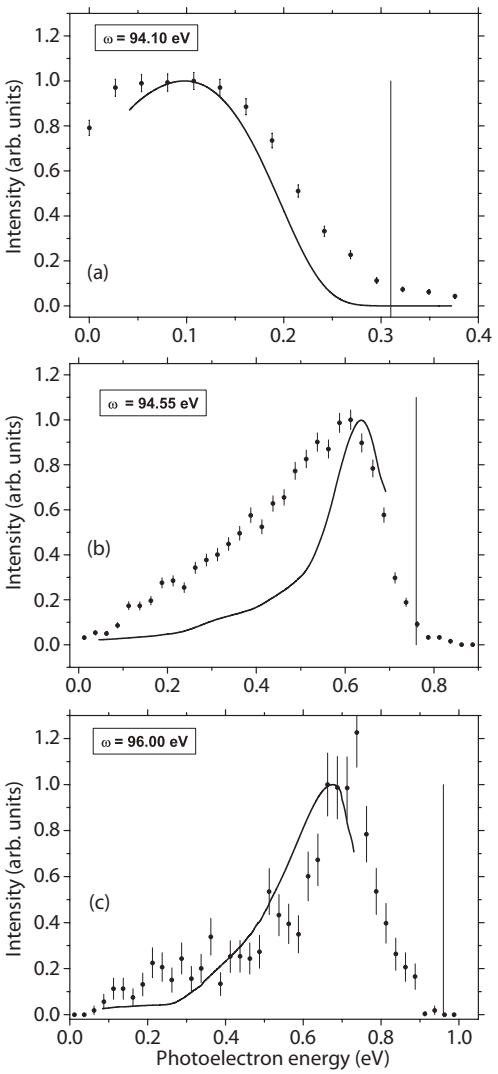

FIG. 1. Experimental and numerical photoelectron spectra for the photon energies of (a) $\omega_1 = 94.10$ eV, (b) $\omega_2 = 94.55$ eV, and (c) $\omega_3 = 96.0$ eV, which are associated with the emission of a slow 0.73-eV Auger electron in the second step of the CDA decay. Dots show experimental data; solid lines show CDA, WKB model, $\Gamma_1 = 88$ meV, $\Gamma_2 = 73$ meV. The vertical line marks the unshifted energy of the photoelectron. For information on the intervals of ΔE_3 see the text.

values for the effective charges of the mean-field potentials obtained by averaging over the electron emission angles. For direct comparison of theory with experiment, we convolved the calculated curves with Gaussians of full width at half maximum (FWHM) = 30 meV to model the experimental resolution. Note that all calculated and experimental curves are normalized to their maximum intensity.

As can be seen from Fig. 1, both the measurements and the calculations reveal strong PCI distortions of the photoelectron line shape. In particular, the intensity maximum of the line shifts to smaller energies, and the line shape becomes asymmetric and shows broadening. For the energy ω_1 the left wing of the line shape shifts to the region of the discrete spectrum (the so-called PCI capture). The shifts of the line-shape maxima for energies ω_1, ω_2, and ω_3 are approximately 0.21,

0.15, and 0.28 eV, respectively. Such nonmonotonic behavior of the PCI shifts can be attributed to strong contributions from the interaction between the slow photoelectron and the slow Auger electron. In comparing with the experiment, we note that while these two electrons are distinguishable in the theory, they may not be distinguishable experimentally when their energies are too similar. This interaction is found to have an opposite sign compared to the interaction between the photoelectron and the ionic field, which varies due to the Auger decays. For the case of ω_2, the energies of the photoelectron and the second Auger electron are close to each other, and their interaction is mostly significant. We note the generally good agreement between the measured and calculated energy distributions, although in the case of ω_2 [cf. Fig. 1(b)] the measured values on the left wing of the line lie notably higher than the calculated values. There is an experimental uncertainty in calibration up to ± 0.05 eV, which may affect Fig. 1(b) particularly.

In Fig. 2 we present experimental photoelectron spectra measured for the same three photon energies, ω_1, ω_2, and ω_3, which are associated with emission of more energetic Auger electrons. In particular, Fig. 2(a) corresponds to the selection of Auger electrons in the interval 7.04–7.53 eV, Fig. 2(b) corresponds to the selection of Auger electrons in the interval 6.60–7.20 eV, and Fig. 2(c) corresponds to the selection of the Auger electrons in the interval 5.31–6.38 eV. In Fig. 2, calculated photoelectron distributions are shown for the case of the CDA decay of the $3d$ vacancy. Our calculations have been carried out accordingly for these three photon energies, ω_1, ω_2, and ω_3, and for the selections of the recorded Auger electrons of energies 7.25–7.75, 6.0–7.60, and 5.31–6.38 eV, respectively. There are a few cascade Auger lines in each of these intervals which are difficult to distinguish experimentally [24,25]. They are associated with different intermediate states involved in the CDA process of Eq. (2). We cannot extract the precise widths of these states from the present experimental data. Hence in our calculations we used an approximation where, for the electrons of the first two intervals, we have used an intermediate state width $\Gamma_2 = 50$ meV, whereas for the electrons of the last interval we used $\Gamma_2 = 60$ meV. These values resulted in the best fit to the experimental data. The same convolution procedure as mentioned above has been adopted for comparison of the experimental and numerical results. Apart from this, in the case of the spectrum associated with the ω_3 energy we have used the theoretical intensity ratio of 0.4 : 0.6 for the $3d_{3/2}$ and $3d_{5/2}$ states.

As can be seen, also all these spectra reflect strong PCI line-shape distortion, including energy shifts of the intensity maxima as well as broadening. As our modeling suggests, both interaction with the ionic field and interaction with the Auger electrons contribute to the PCI distortion of the photoelectron distribution. For the lower photon energies [cf. Figs. 2(a) and 2(b)] the calculated curves are shifted slightly towards the lower-kinetic-energy side in comparison to the measured spectra. The generally good agreement suggests that our theoretical model of the CDA decay allows us to describe the measured spectra adequately.

Figure 3 shows photoelectron spectra which are primarily associated with the DDA processes. In particular, Fig. 3(a) represents the measured and calculated spectrum for photon energy ω_1, where the photoelectron is selected in coincidence

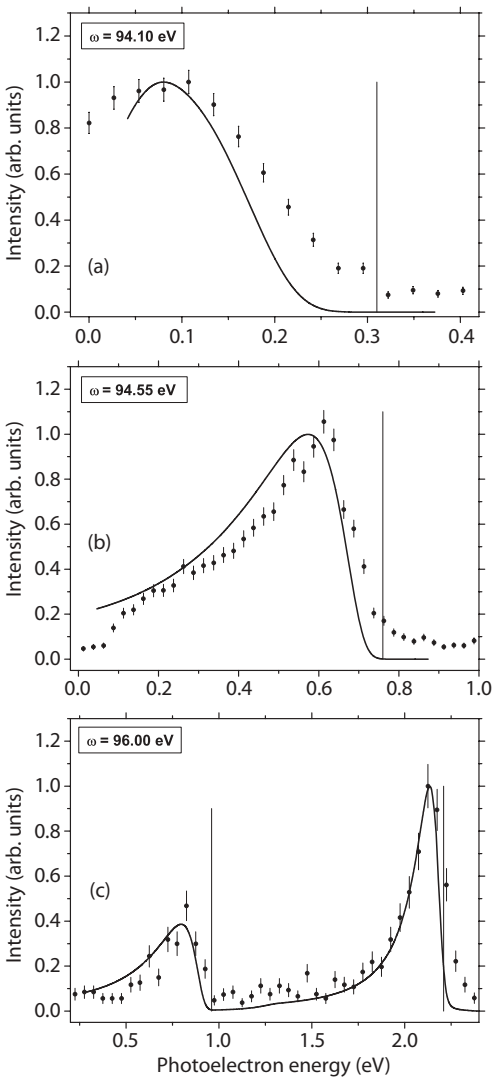

FIG. 2. Experimental and numerical photoelectron spectra for the photon energies of (a) $\omega_1 = 94.10$ eV, (b) $\omega_2 = 94.55$ eV, and (c) $\omega_3 = 96.0$ eV, respectively, which are associated with emission of more energetic Auger electrons. Dots show experimental data; solid lines show CDA, WKB model, $\Gamma_1 = 88meV$, $\Gamma_2 = 50$ meV for cases (a) and ((b) and $\Gamma_2 = 60$ meV for case (c). The vertical line marks the unshifted energy of the photoelectron; for information on the intervals of ΔE_2 see the text.

with Auger electrons of the energy interval 1.45–2.1 eV, Fig. 3(b) shows the corresponding case for the ω_2 photon energy and the Auger energy interval of 1.45–1.95 eV, and Fig. 3(c) reflects the case for the ω_3 photon energy and the Auger energy interval of 2.80–3.83 eV. All theoretical curves are calculated using Eq. (4) and a width for the $3d$ inner-shell vacancy of $\Gamma = 88$ meV. For comparison of theory with experiment, we convolved again the calculated curves with Gaussians of FWHM = 30 meV.

Akin to the cases discussed above, the measured and calculated spectra reveal strong PCI distortion, where the maxima of the line shapes are shifted to the low-kinetic-energy side and where the line shapes become broad and asymmetrical. Due to the small excess energy above the ionization threshold the main contribution to the PCI distortion

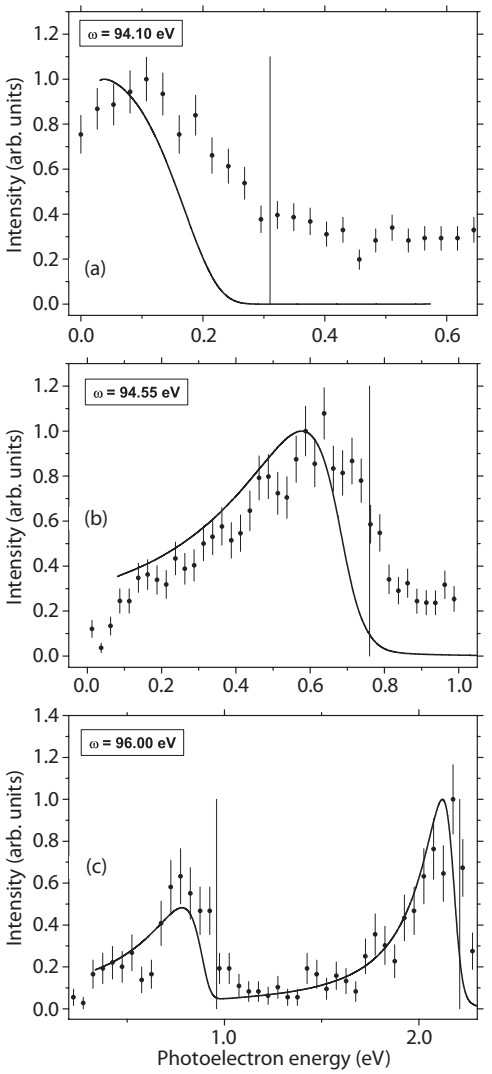

FIG. 3. Experimental and numerical photoelectron spectra which are primarily associated with the DDA processes. Dots show experimental data; solid lines show DDA, WKB model, $\Gamma = 88$ meV. The vertical line marks the unshifted energy of the photoelectron; for information on the intervals of ΔE_2 see the text.

comes from interaction between the slow photoelectron and the ionic field, which varies during the course of the DDA decay. However, the interaction of the photoelectron with the two Auger electrons of energies ∼2 and ∼13 eV is quite significant. Again, we find a good agreement between the measured and calculated line shapes for the case of the ω_3 photon energy. For the cases of the ω_1 and ω_2 energies the calculated curves are shifted towards the low-kinetic-energy side of the spectra by approximately 0.1 eV. Apart from this, the measured distribution for the ω_1 energy shows nonzero intensity on the high-kinetic-energy side of the line, where the theory predicts very low electron yield. This discrepancy may be attributed to background contributions to the measured spectra, for instance, secondary electron emission from the impact of energetic electrons on metal surfaces.

V. CONCLUSION

Two powerful tools, multielectron coincidence spectroscopy based on a magnetic bottle and a semiclassical approach, have been used to investigate low-kinetic-energy $3d$ photoelectron spectra of krypton which are affected by the double Auger decay of this inner-shell vacancy. Both the measurements and calculations revealed strong distortion of the photoelectron line shapes. This distortion is due to PCI associated with the processes of DA decay. The shifts, broadening, and asymmetry of the lines depend on the velocities of the escaping electrons, the characteristics of the Auger decay, and the properties of the intermediate states involved in the decay process. Generally good agreement between the measured and calculated energy distributions demonstrates the validity of the approach used and suggests the applicability of this method to low-energy photoelectron spectra of other atomic and molecular systems.

ACKNOWLEDGMENTS

This work has been financially supported by the Swedish Research Council (VR), the Göran Gustafsson Foundation (UU/KTH), and the Knut and Alice Wallenberg Foundation, Sweden. S.S. acknowledges financial support from the Wenner-Gren Foundations, Sweden. This work was also supported by the European Community Research Infrastructure Action under the FP6 "Structuring the European Research Area" Programme (through the Integrated Infrastructure Initiative "Integrating Activity on Synchroton and Free Electron Laser Science," Contract No. R II 3-CT-2004-506008).

[1] M. Yu. Kuchiev and S. A. Sheinerman, Sov. Phys. Usp. **32**, 569 (1989).
[2] V. Schmidt, Rep. Prog. Phys. **55**, 1483 (1992).
[3] T. A. Carlson and M. O. Krause, Phys. Rev. Lett. **14**, 390 (1965).
[4] T. A. Carlson and M. O. Krause, Phys. Rev. Lett. **17**, 1079 (1966).
[5] J. H. D. Eland, O. Vieuxmaire, T. Kinugawa, P. Lablanquie, R. I. Hall, and F. Penent, Phys. Rev. Lett. **90**, 053003 (2003).
[6] J. Viefhaus, M. Braune, S. Korica, A. Reinköster, D. Rolles, and U. Becker, J. Phys. B **38**, 3885 (2005).
[7] F. Penent, J. Palaudoux, P. Lablanquie, L. Andric, R. Feifel, and J. H. D. Eland, Phys. Rev. Lett. **95**, 083002 (2005).
[8] J. H. D. Eland, Adv. Chem. Phys. **141**, 103 (2009).
[9] T. Hayaishi, E. Murakami, A. Yagishita, F. Koike, Y. Morioka, and J. E. Hansen, J. Phys. B **21**, 3203 (1988).
[10] T. Hayaishi, A. Yagishita, E. Shigemasa, E. Murakami, and Y. Morioka, J. Phys. B **23**, 4431 (1990).

[11] T. Hayaishi, E. Murakami, Y. Morioka, E. Shigemasa, A. Yagishita, and F. Koike, J. Phys. B **27**, L115 (1994).
[12] H. Kjeldsen, T. D. Thomas, P. Lablanquie, M. Lavollée, J. H. D. Eland, F. Penent, M. Hochlaf, and R. I. Hall, J. Phys. B **29**, 1689 (1996).
[13] T. Hayaishi, T. Tanaka, H. Yoshii, E. Murakami, E. Shigemasa, A. Yagishita, F. Koike, and Y. Morioka, J. Phys. B **32**, 1507 (1999).
[14] T. Hayaishi, Y. Fujita, M. Izumisawa, T. Tanaka, E. Murakami, E. Shigemasa, A. Yagishita, and Y. Morioka, J. Phys. B **33**, 37 (2000).
[15] T. Hayaishi, T. Matsui, H. Yoshii, A. Higurashi, E. Murakami, A. Yagishita, T. Aoto, T. Onuma, and Y. Morioka, J. Phys. B **35**, 141 (2002).
[16] T. Matsui, H. Yoshii, A. Higurashi, E. Murakami, T. Aoto, T. Onuma, Y. Morioka, A. Yagishita, and T. Hayaishi, J. Phys. B **35**, 3069 (2002).
[17] P. Lablanquie, S. Sheinerman, F. Penent, R. I. Hall, M. Ahmad, Y. Hikosaka, and K. Ito, Phys. Rev. Lett. **87**, 053001 (2001).
[18] P. Lablanquie, S. Sheinerman, F. Penent, R. I. Hall, M. Ahmad, T. Aoto, Y. Hikosaka, and K. Ito, J. Phys. B **35**, 3265 (2002).
[19] S. Sheinerman, P. Lablanquie, F. Penent, Y. Hikosaka, T. Kaneyasu, E. Shigemasa, and K. Ito, J. Phys. B **43**, 115001 (2010).
[20] F. Koike, Phys. Lett. A **193**, 173 (1994).
[21] S. A. Sheinerman, J. Phys. B **27**, L571 (1994).
[22] S. A. Sheinerman, J. Phys. B **31**, L361 (1998).
[23] L. Gerchikov and S. Sheinerman, Phys. Rev. A **84**, 022503 (2011).
[24] E. Andersson, S. Fritzsche, P. Linusson, L. Hedin, J. H. D. Eland, J.-E. Rubensson, L. Karlsson, and R. Feifel, Phys. Rev. A **82**, 043418 (2010).
[25] J. Palaudoux, P. Lablanquie, L. Andric, K. Ito, E. Shigemasa, J. H. D. Eland, V. Jonauskas, S. Kučas, R. Karazija, and F. Penent, Phys. Rev. A **82**, 043419 (2010).
[26] Y. Hikosaka, P. Lablanquie, F. Penent, T. Kaneyasu, E. Shigemasa, R. Feifel, J. H. D. Eland, and K. Ito, Phys. Rev. Lett. **102**, 013002 (2009).
[27] K. J. S. Sawhney, F. Senf, M. Scheer, F. Schafers, J. Bahrdt, A. Gaupp, and W. Gudat, Nucl. Instrum. Methods Phys. Res., Sect. A **390**, 395 (1997).
[28] E. Andersson, M. Stenrup, J. H. D. Eland, L. Hedin, M. Berglund, L. Karlsson, Å. Larson, H. Ågren, J.-E. Rubensson, and R. Feifel, Phys. Rev. A **78**, 023409 (2008).
[29] http://www.bessy.de.
[30] G. C. King, M. Tronc, F. H. Read, and R. C. Bradford, J. Phys. B **10**, 2479 (1977).
[31] L. O. Werme, T. Bergmark, and K. Siegbahn, Phys. Scr. **6**, 141 (1972).
[32] H. Aksela, S. Aksela, and H. Pulkkinen, Phys. Rev. A **30**, 2456 (1984).
[33] M. Jurvansuu, A. Kivimäki, and S. Aksela, Phys. Rev. A **64**, 012502 (2001).